Received: 23 August 2019 | Revised: 10 February 2020 | Accepted: 25 March 2020

DOI: 10.1002/qj.3799

Quarterly Journal of the Royal Meteorological Society RMetS

RESEARCH ARTICLE

Impact of the Pacific Meridional Mode on landfalling tropical cyclone frequency in China

Si Gao[1,2] | Langfeng Zhu[3] | Wei Zhang[4] | Xinyong Shen[2,3]

[1]School of Atmospheric Sciences, and Guangdong Province Key Laboratory for Climate Change and Natural Disaster Studies, Sun Yat-sen University, Zhuhai, China

[2]Southern Marine Science and Engineering Guangdong Laboratory (Zhuhai), Zhuhai, China

[3]Key Laboratory of Meteorological Disaster, Ministry of Education, and Collaborative Innovation Center on Forecast and Evaluation of Meteorological Disaster, Nanjing University of Information Science and Technology, Nanjing, China

[4]IIHR-Hydroscience and Engineering, The University of Iowa, Iowa City, Iowa

Correspondence
W Zhang, IIHR-Hydroscience and Engineering, The University of Iowa, Iowa City, IA 52242, USA.
Email: wei-zhang-3@uiowa.edu

Funding information
National Natural Science Foundation of China, Grant/Award Number: 41930967, 41575078, 41975054.

Abstract

This study identifies a significant positive correlation between the Pacific Meridional Mode (PMM) index and frequency of tropical cyclones (TCs) landfalling in China during peak TC season (June–November) of the period 1977–2018. This interannual association is independent of two types of El Niño–Southern Oscillation. Large-scale circulation over the western North Pacific (WNP) modulated by PMM can affect TC genesis location/frequency and steering flow that directly determine TC landfalls in China. During the positive PMM phase, anomalous off-equatorial heating over the eastern North Pacific can induce anomalous low-level cyclonic circulation and upper-level anticyclonic circulation over most of the main development region in the WNP, as a Gill-type Rossby wave response. The resultant larger low-level relative vorticity and weaker vertical wind shear are conducive to the formation of more TCs over the main development region. The anomalous easterly steering flow in the north flank of the anomalous low-level cyclonic circulation is favourable for more TCs moving westward/northwestward and making landfall in China. The physical mechanism for the impact of PMM on large-scale circulation over the WNP is verified by numerical experiments using the Community Atmospheric Model. The PMM index is demonstrated to be a crucial predictor for landfalling TC frequency in China in statistical seasonal prediction models.

KEYWORDS

China, interannual variation, Pacific Meridional Mode, tropical cyclone landfall

1 | INTRODUCTION

Tropical cyclones (TCs) making landfall are the most destructive natural disasters affecting the most economically developed and highly populated coastal regions in China. The associated heavy rains, storm surges, and strong winds have the potential to cause massive casualties and economic losses. In an average year during 1983 to 2006, there were seven TCs making landfall in China, leading to 472 deaths and direct economic losses of 28.7 billion yuan (Zhang *et al.*, 2009). Landfalling TC frequency in China exhibits strong interannual variability (e.g. Zhou and Lu, 2019). A better understanding of the interannual relationship between TC landfalls in China and climate variations is of great significance in mitigating TC hazards.

The frequency of TCs landfalling in China on the interannual time-scale is closely related to the El Niño–Southern Oscillation (ENSO). More TCs make

landfall in south China in La Niña years, owing to a westward shift in genesis location and stronger western North Pacific (WNP) subtropical high (Elsner and Liu, 2003; Liu and Chan, 2003; Wu *et al.*, 2004; Zhang *et al.*, 2012; 2016a). Wang *et al.* (2013) emphasized the strong modulation of the WNP subtropical high on TC landfalls in China; this relationship was also well produced by the UK Met Office Global Seasonal forecasting system version 5 (Camp *et al.*, 2019). Yu *et al.* (2017) suggested that a northward shift of the East Asian subtropical westerly jet is connected with anomalous easterly steering flow over the coastal area of east China, which favours a larger number of TC landfalls in China during boreal summer. Gao *et al.* (2018a) found a negative correlation between tropical North Atlantic (TNA) sea-surface temperature (SST) and frequency of TCs making landfall in China during the peak TC season. Cold TNA SST anomaly favours genesis of more TCs in the South China Sea, the western Philippine Sea, and the eastern part of WNP; these TCs move towards China by following climatological mean steering flow. Wang and Chen (2018a) revealed a negative association of boreal spring SST gradient (SSTG) between the tropical Indian Ocean and the western Pacific warm pool with summer TC landfalls in China. A negative spring SSTG can induce anomalous low-level cyclone and weaker vertical wind shear over a large portion of the WNP, which increase TC genesis frequency, and the accompanying easterly steering flow anomalies over coastal China result in more TC landfalls in China. Wang and Chen (2018b) identified a negative relationship between the onset date of the South China Sea summer monsoon and peak-season TC landfalls in China. Early onset of the South China Sea summer monsoon is accompanied by a strong monsoon trough and anomalous low-level cyclone around Luzon Island which favour TC genesis in the western part of the WNP, and the associated easterly steering flow leads more TCs to make landfall in southeast China. Zhang *et al.* (2019) showed that the frequency of TCs landfalling in southern China is mainly influenced by the surrounding easterly steering flow closely related to the WNP subtropical high.

The Pacific Meridional Mode (PMM) is an atmosphere–ocean coupled phenomenon with strong signals on similar interannual time-scales to ENSO. The spatial pattern of PMM shows the coupling of a meridional SST gradient and a cross-gradient surface airflow; this is obtained with maximum covariance analysis on detrended fields of SST and surface wind after removing the canonical ENSO signal and seasonal cycle (Chiang and Vimont, 2004). Although the PMM index is significantly correlated with the ENSO modoki index, which suggests that the two climate modes are not strictly independent (Stuecker, 2018), PMM and ENSO modoki are likely two different phenomena. Besides their different spatial patterns, they mature in different periods (boreal spring for PMM and boreal winter for ENSO modoki). PMM has positive impacts on the occurrence of WNP TCs (Zhang *et al.*, 2016b; Zhan *et al.*, 2017; Wu *et al.*, 2018) and intense TCs (Gao *et al.*, 2018b), and can be used to predict the frequency of TCs (Zhang and Villarini, 2019) and landfalling TCs over the WNP in a statistical–dynamical framework (Zhang *et al.*, 2017). A positive PMM can shift the mean TC genesis location eastward (Hong *et al.*, 2018).

Although the impacts of PMM on WNP TC activity have gained much attention, no studies have reported its influence on TC landfalls in China and other countries of East Asia. Owing to the serious destructiveness of landfalling TCs and the challenge of predicting the frequency of TC landfalls, it is highly desirable to discover whether and how PMM modulates landfalling TC frequency over the WNP. We will accomplish the objectives using observational analysis and numerical experiments. Section 2 describes data and methods. The statistical relationship between PMM and TC landfalls over the WNP is investigated in Section 3. Section 4 examines the possible mechanisms for the impact of PMM on TC landfalls in China. Section 5 gives a discussion. Concluding remarks are presented in Section 6.

2 | DATA AND METHODS

The 6-hourly TC position and intensity are obtained from the China Meteorological Administration (CMA) best-track data (Ying *et al.*, 2014). We use the data over the satellite era from 1977 to 2018. A detection algorithm (details can be found in Gao *et al.*, 2018a) is used to identify the frequency of landfalling TCs in four subregions: China, Korea and Japan, Vietnam, and the Philippines. Figure 1 shows the coastal lines of the four subregions and the entire East Asia. TC landfalls in Taiwan are not counted as landfalls in China but counted as landfalls in the entire East Asia in this study. Note that multiple landfalls within a region for an individual TC is only counted as one landfall in that region. Figure 2 indicates monthly climatology of landfalling TC frequency in each subregion and the entirety of East Asia. Among the four subregions, China suffers the most frequent TC strikes. TC landfalls mainly occur in the peak TC season (June–November, JJASON), during which climatological mean frequencies of TCs landfalling in China, Korea and Japan, Vietnam, the Philippines, and the entire East Asia are 7.2, 4.8, 2.6, 6.0, and 17.2, respectively. We therefore focus on the period of JJASON in this study.

Monthly atmospheric variables are acquired from the National Centers for Environmental Prediction

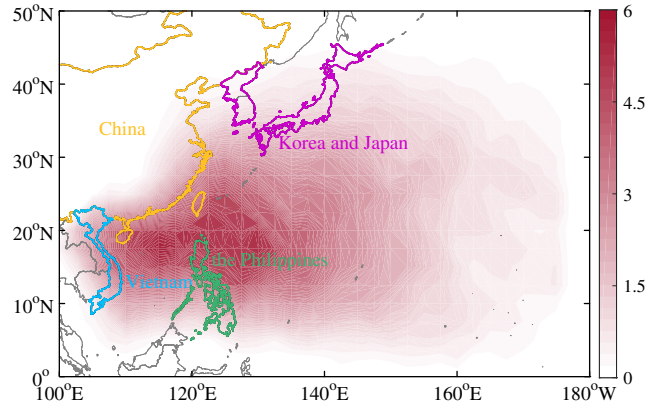

FIGURE 1 Four defined landfalling subregions in East Asia: China, Korea and Japan, Vietnam, and the Philippines. Landfalling TCs in Taiwan are not counted in China but counted in the entire East Asia in this study. Shading denotes track density during 1977–2018 [Colour figure can be viewed at wileyonlinelibrary.com]

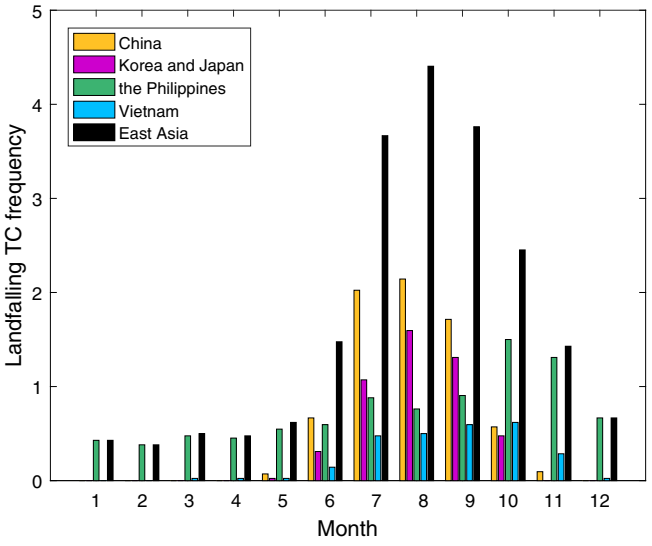

FIGURE 2 Monthly climatology of landfalling TC frequency in each subregion and the entirety of East Asia during 1977–2018 [Colour figure can be viewed at wileyonlinelibrary.com]

(NCEP)/National Center for Atmospheric Research (NCAR) Reanalysis data at 2.5° resolution (Kalnay *et al.*, 1996). Monthly interpolated outgoing long-wave radiation (OLR) data at 2.5° resolution (Liebmann and Smith, 1996), PMM SST index (hereafter PMM index), and Niño 3.4 index are obtained from the Physical Sciences Division (PSD) of the National Oceanic and Atmospheric Administration (NOAA)/Earth System Research Laboratory (ESRL). The Niño 3.4 index is used to define canonical ENSO events since the Niño 3.4 region is the key region for coupled ocean–atmosphere interactions for canonical ENSO (Trenberth, 1997), and the PMM SST index is used to define the PMM phases (Chiang and Vimont, 2004).

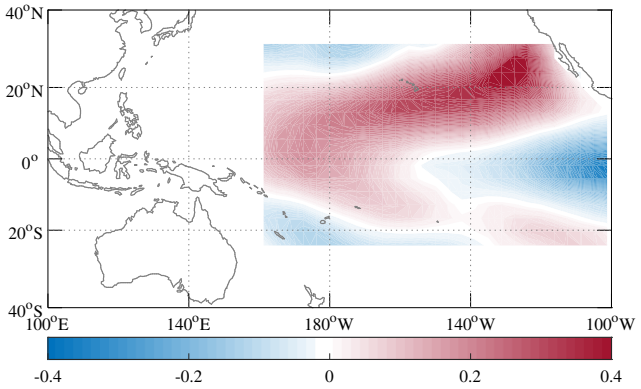

FIGURE 3 The differences in prescribed SST (K) between the PPMM and CTRL experiment with CAM-5.3 (PPMM minus CTRL) [Colour figure can be viewed at wileyonlinelibrary.com]

Monthly SST data at 1° resolution are acquired from the NOAA Extended Reconstructed Sea Surface Temperature (ERSST) version 4 (Huang *et al.*, 2015). The ENSO Modoki index (EMI) is provided by the Japan Agency for Marine-Earth Science and Technology (JAMSTEC). These atmospheric and oceanic variables are detrended first to only investigate interannual variations.

To verify the physical mechanisms for impact of PMM on large-scale circulation, which directly controls frequency of TC landfalls, we use the latest version 5.3 of the National Center for Atmospheric Research (NCAR) Community Atmospheric Model (CAM-5.3: Neale *et al.*, 2012) to perform perturbation experiments. CAM-5.3 was released as an atmospheric component for version 1.2 of the Community Earth System Model (CESM: Hurrell *et al.*, 2013). CAM-5.3 with T31 horizontal resolution (3.75° × 3.75°) and 26 vertical levels is used to conduct two experiments; one is prescribed with the observed climatological SST (CTRL experiment), and the other with the regressed SST anomalies onto the PMM index (Figure 3) added to the observed climatological SST during JJASON in the PMM region and the same as the CTRL experiment elsewhere (PPMM experiment). Both CTRL and PPMM experiments were integrated for 100 years. We compare the differences between the PPMM and CTRL experiments (PPMM minus CTRL) during the last 80 years, which represents the changes forced by off-equatorial SST warming related to the positive PMM phase.

3 | STATISTICAL RELATIONSHIP BETWEEN PMM AND TC LANDFALLS

Table 1 shows the correlation coefficients between the PMM index and the frequency of TCs landfalling in each subregion and the entirety of East Asia during JJASON of

TABLE 1 Correlation coefficients (r) of the PMM index with landfalling TC frequency in each subregion and the entirety of East Asia during JJASON of the period 1977–2018

Region	China	Korea and Japan	The Philippines	Vietnam	East Asia
r	0.45[a]	0.14	0.17	0.17	0.52[a]

[a] Significance at the 0.01 level.

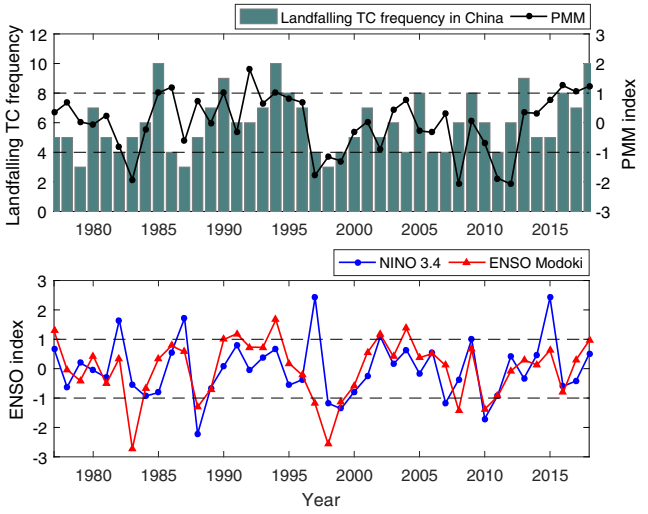

FIGURE 4 Time series of the frequency of TCs landfalling in China (black line) and normalized PMM index (green bar), ENSO Modoki index (red line) and Niño 3.4 index (blue line) during JJASON of 1977–2018 [Colour figure can be viewed at wileyonlinelibrary.com]

the period 1977–2018. The PMM index is significantly correlated with TC landfalls in the subregion of China only, and it dominates the significant correlation of PMM with TC landfalls in the whole East Asia. We thus only discuss the relationship of PMM with TC landfalls in China hereafter. Figure 4 shows the time series of landfalling TC frequency in China and normalized climate indices (Niño 3.4, PMM, and ENSO Modoki) during JJASON of the period 1977–2018. Following Gao *et al.* (2018b), we first select typical years in the positive and negative PMM phases and typical canonical El Niño and La Niña years using one standard deviation of the normalized time series of PMM and Niño 3.4 indices in Figure 4. Since strong PMM and canonical ENSO events may coexist in an individual year, the typical canonical El Niño and La Niña years are then excluded from the typical years in two PMM phases to remove the ENSO effect. Accordingly, 8 years in the positive PMM phase (i.e. 1985, 1986, 1990, 1992, 1994, 2016, 2017 and 2018) and 4 years in the negative PMM phase (i.e. 1983, 2008, 2011 and 2012) are selected to perform WNP TC statistics. Following Gao *et al.* (2018b), the typical ENSO Modoki years are not excluded as PMM and ENSO Modoki are not strictly independent (Stuecker, 2018). Due to a small number of samples, the interpretation of results may be limited, therefore we further conduct numerical experiments to verify the proposed physical mechanisms.

The PMM index and landfalling TC frequency in China have a significant correlation coefficient of 0.45 ($p < .01$). The partial correlation coefficients between them by controlling the Niño 3.4 and ENSO Modoki indices are 0.45 ($p < .01$) and 0.34 ($p < .05$), respectively; Both are statistically significant. Landfalling TC frequency in China has a weak correlation of −0.11 with the Niño 3.4 index; this is not surprising because canonical ENSO merely modulates TC landfalls in China during boreal autumn and has no significant correlation with TC landfalls in either south China, east China, or the entire China during boreal summer (Elsner and Liu, 2003; Liu and Chan, 2003; Wu *et al.*, 2004; Zhang *et al.*, 2012). Landfalling TC frequency in China shows a significant correlation of 0.34 ($p < .05$) with EMI, consistent with Zhang *et al.* (2012). The results indicate that both PMM and ENSO Modoki can affect landfalling TC frequency in China during JJASON. Indeed, the coexistence of positive phase of PMM and ENSO Modoki in neutral or weak state of canonical ENSO can significantly enhance (i.e. 1990 and 1994, with 9 and 10 landfalls, respectively) TC landfalls in China. However, there are 5 years in neutral or weak state of two types of ENSO during which the PMM index shows strong association with TC landfalls in China. Ten, 8 and 10 TCs made landfall in China in 1985, 2016 and 2018 that were in the positive PMM phase and 4 and 6 TCs made landfall in China in 2011 and 2012 that were in the negative PMM phase. This suggests an important role of PMM in modulating the frequency of TC landfalls in China, which could be independent of two types of ENSO event.

Table 2 shows statistics for the frequency of all WNP TCs (i.e. lifetime maximum intensity ≥17.2 $m \cdot s^{-1}$) and TCs landfalling in China during JJASON of two PMM phases. The mean frequency of all WNP TCs in the positive PMM phase is significantly higher than that in the negative phase at the 0.01 level (27.1 vs. 20.3), in line with previous studies (Zhang *et al.*, 2016b; Zhan *et al.*, 2017; Wu *et al.*, 2018). On average, there are 8.0 and 5.3 ($p < .01$) TCs landfalling in China, corresponding to 29.5 and 25.9% ($p = .46$) of all WNP TCs making landfall in China during the positive and negative PMM phases, respectively. The significantly larger number of total TC frequency and landfalling TC frequency in China are consistent with their rankings during the study period. It is thus suggested that the higher frequency of TCs landfalling in China is partially ascribed to the higher frequency of all WNP TCs during the positive PMM phase compared to the negative PMM phase. However, there must be other physical

TABLE 2 Total and average (in parentheses) frequency of all WNP TCs and TCs landfalling in China during JJASON as well as rankings of their annual numbers in the 42-year period during positive and negative PMM phases

Parameter	Negative PMM phase (4 years)	Positive PMM phase (8 years)
Frequency of all WNP TCs	**81 (20.3)**	**217 (27.1)**
Ranking of WNP TC frequency	19, 30, 34, 34	1, 2, 6, 6, 8, 8, 15, 15
Frequency of TCs landfalling in China	**21 (5.3)**	**64 (8.0)**
Ranking of landfalling TC frequency in China	16, 16, 23, 32	1, 1, 1, 4, 6, 10, 16, 32
Ratio of TCs landfalling in China to all WNP TCs	25.9%	29.5%

Note: Ratios of TCs landfalling in China to all WNP TCs are also shown. Bold values indicate significance above the .05 level based on Student's *t*-test.

reasons why these extra TCs during the positive PMM phase prefer to make landfall only in China, which will be discussed in the next section.

4 | POSSIBLE MECHANISMS

It is widely accepted that TC genesis frequency/location and steering flow directly determine TC landfalls in a specific area (e.g. Liu and Chan, 2003; Wu *et al.*, 2004; Zhang *et al.*, 2012; Zhou *et al.*, 2018; Gao *et al.*, 2018a). In this section, we first find out the hot spots of TC genesis modulated by PMM, although previous studies (Zhang *et al.*, 2016b; Gao *et al.*, 2018b) have revealed the relationship between PMM and WNP TC genesis frequency. We then interpret the impacts of PMM on TC landfalls in China combining TC track based on PMM-modulated steering flow. All the regressions below are obtained after removing the regressed fields onto the Niño 3.4 index to exclude the linear effect of canonical ENSO. Figure 5 indicates regressions of genesis density and track density of all WNP TCs onto the PMM index during JJASON as well as the prevailing tracks of TCs landfalling in China during the positive PMM phase. Compared to the negative PMM phase, significantly more TCs form over two regions (140°–150°E, 10°–20°N) and (120°–130°E, 15°–25°N) during the positive PMM phase (Figure 5a). These TCs mainly follow two groups of tracks: a fraction of them recurve and pose no threat to land (tracks are not shown), and the others move west-northwestward and make landfall in southeast and south China (black arrows in Figure 5b). The latter contributes to significantly more TC landfalls in China during the positive PMM phase than the negative PMM phase.

Similar to previous studies (e.g. Camargo *et al.*, 2007; Gao *et al.*, 2018a), we use genesis potential index (GPI: Emanuel and Nolan, 2004) to investigate PMM effects on TC genesis. Figure 6 shows regression of GPI onto the PMM index during JJASON. The larger GPI values are in good agreement with higher genesis density (Figure 5a) during the positive PMM phase, indicating that GPI is suitable for diagnosing TC genesis during different PMM phases. Four components of GPI, that is, 850 hPa relative vorticity, 600 hPa relative humidity, maximum potential intensity (MPI: Emanuel, 1988), and 850–200 hPa vertical wind shear are further examined. Figure 7 shows regressions of the four variables onto the PMM index during JJASON. Compared to the negative PMM phase, significantly larger low-level relative vorticity (Figure 7a) and weaker wind shear (Figure 7d) are responsible for the genesis of more TCs during the positive PMM phase, consistent with previous studies (Zhang *et al.*, 2016b; Gao *et al.*, 2018b).

Figure 8 indicates regression of steering flow (layer mean winds from 850 to 500 hPa: Chan and Gray, 1982;

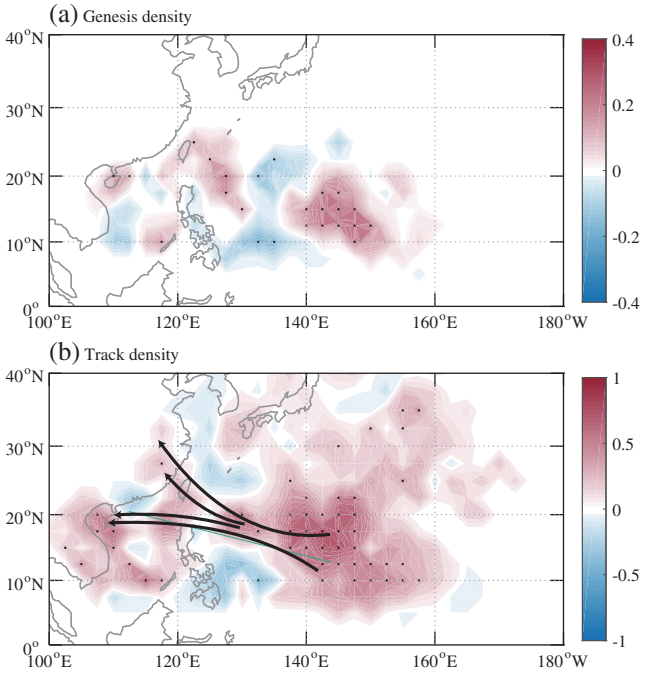

FIGURE 5 Regressions of (a) genesis density and (b) track density onto the PMM index during JJASON after removing the Niño 3.4 signal. Values above the 0.1 significance level are stippled. The arrows denote prevailing tracks of a larger number of TCs landfalling in China during the positive PMM phase compared to the negative PMM phase [Colour figure can be viewed at wileyonlinelibrary.com]

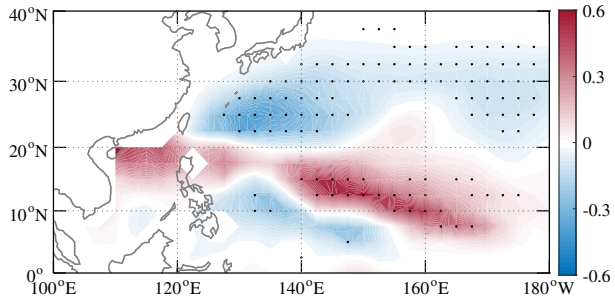

FIGURE 6 Regressions of GPI during JJASON after removing the Niño 3.4 signal. Values above the 0.1 significance level are stippled [Colour figure can be viewed at wileyonlinelibrary.com]

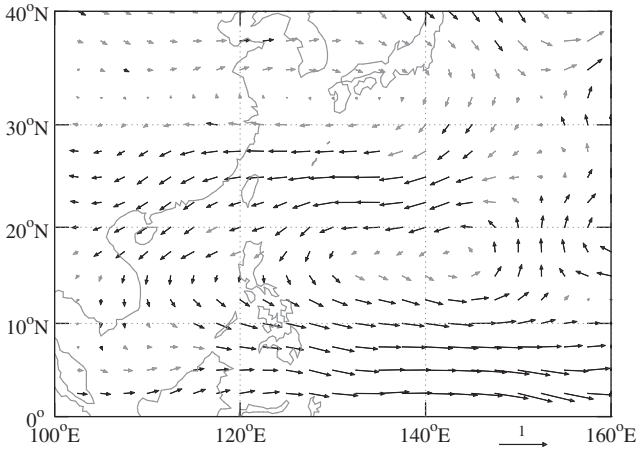

FIGURE 8 Regression of steering flow ($m \cdot s^{-1}$) onto the PMM index during JJASON after removing the Niño 3.4 signal. Black vectors exceed the 0.1 significance level

Velden and Leslie, 1991) onto the PMM index during JJASON. There is a significant cyclonic flow pattern over the western part of WNP and southern China. JJASON mean steering flow and location of the WNP subtropical high during two PMM phases and the difference in steering flow between them are also shown in Figure 9. During the positive PMM phase, northwestward TC tracks toward Taiwan and southeast China as well as westward TC tracks toward south China (Figure 5b) are generally consistent with southwesterly/easterly steering flow along their paths (Figure 9a); the anomalous easterly and northeasterly steering flows over southern China (Figure 8) favour TCs moving more westward and making landfall in southern China; in addition, a weaker WNP subtropical high (Figure 9a) favours a part of the TCs that form in the region (140°–150°E, 10°–20°N) recurving northeastward. During the negative PMM phase, the WNP subtropical high is stronger, while the associated easterly steering flow is strengthened at 0–15°N and the associated westerly steering flow is strengthened at 20–30°N (Figures 8 and 9c). Meanwhile, TC geneses are overall suppressed (Figure 5a); both TC genesis and steering flow are therefore unfavourable for TC landfalls in China.

Figure 10 shows the regressions of SST, 850 and 200 hPa winds, and OLR (as a proxy for atmospheric heating) onto the PMM index during JJASON. Anomalous cyclonic flow in the lower troposphere (Figure 10a) and anomalous anticyclonic flow in the upper troposphere (Figure 10b) prevail over most of the WNP during the positive PMM phase. The flow patterns result in larger low-level relative

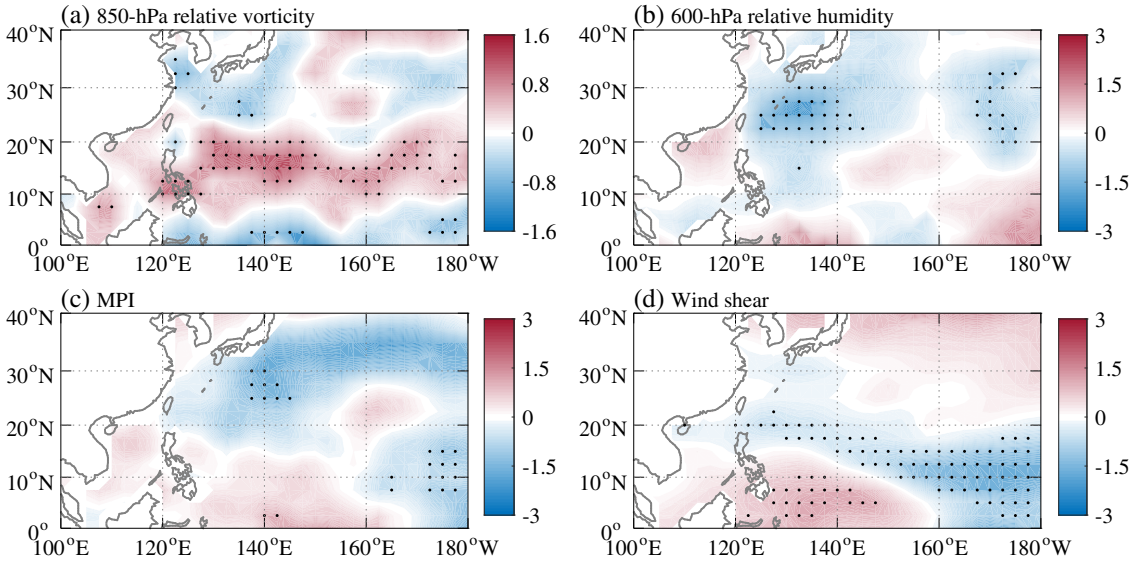

FIGURE 7 Regressions of (a) 850 hPa relative vorticity (10^{-6} s^{-1}), (b) 600 hPa relative humidity (%), (c) MPI ($m \cdot s^{-1}$), and (d) 850–200 hPa vertical wind shear ($m \cdot s^{-1}$) onto the PMM index during JJASON after removing the Niño 3.4 signal. Values above the 0.1 significance level are stippled [Colour figure can be viewed at wileyonlinelibrary.com]

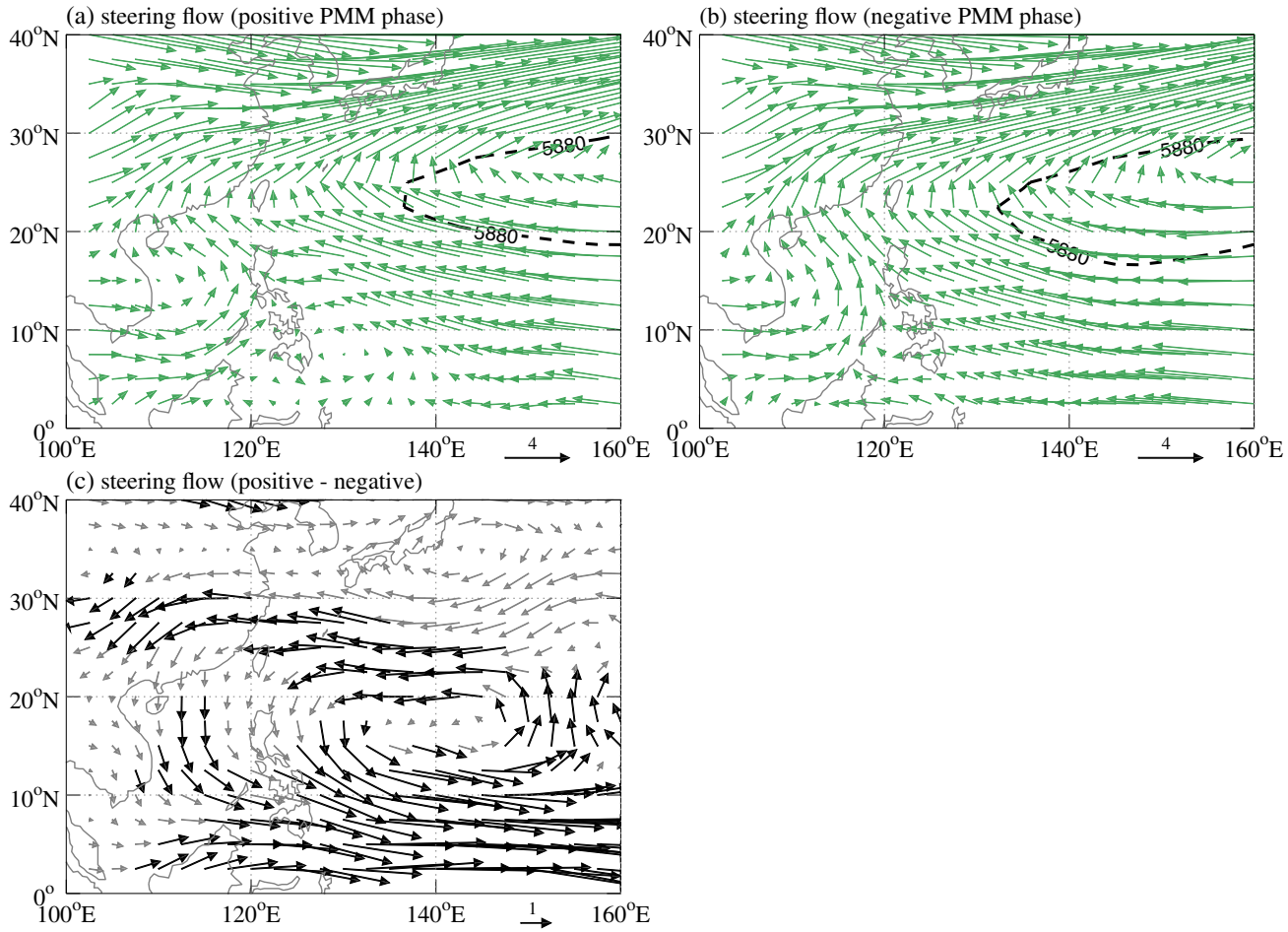

FIGURE 9 JJASON mean steering flow (vector, $m \cdot s^{-1}$) and location of WNP subtropical high (denoted by the 5,880 gpm contour) during (a) the positive and (b) the negative PMM phase, and (c) the difference in steering flow between them. Black vectors show winds significant above the 0.1 level [Colour figure can be viewed at wileyonlinelibrary.com]

vorticity and weaker wind shear over the main development region (Figure 7a,d); the latter is because the prevailing upper-level westerlies and low-level easterlies are both weakened. Note that there are almost no significant upper-level westerlies in the East Asian subtropical westerly jet region. This suggests that PMM cannot modulate the subtropical westerly jet, although previous studies (e.g. Yu *et al.*, 2017) showed that the East Asian subtropical westerly jet has the potential to influence TC landfalls in China.

The anomalous flow patterns (Figure 10) are plausibly a Gill-type Rossby wave response (Gill, 1980) to anomalous off-equatorial heating (Figure 10b) associated with warmer SST during the positive PMM phase (Figure 10a). To verify this, we conduct the perturbation experiments using CAM-5.3 (see details in Section 2). The differences in OLR and wind fields at 850 and 200 hPa during JJASON between the PPMM and CTRL experiments (Figure 11) strongly resemble their regressed patterns onto the PMM index in Figure 10. The difference in steering flow (layer mean winds from 850 to 500 hPa) during JJASON between the PPMM and CTRL experiments (Figure 12) also resembles its regressed pattern onto the PMM index over the western part of WNP in Figure 8, which is responsible for the westward/northwestward track of TCs making landfall in China. The Gill-type response to the off-equatorial heating related to SST warming during the positive PMM phase is thus reasonably well reproduced by the CAM-5.3 experiments. This is basically consistent with the modelling studies using other numerical models (Zhang *et al.*, 2016b; Gao *et al.*, 2018b) and further demonstrates the robustness of the modulation of PMM on large-scale circulations over the WNP, which most likely leads to anomalous TC landfalls in China.

5 | DISCUSSION

Given PMM is not strictly independent of ENSO Modoki, one may doubt the usefulness of the PMM index in

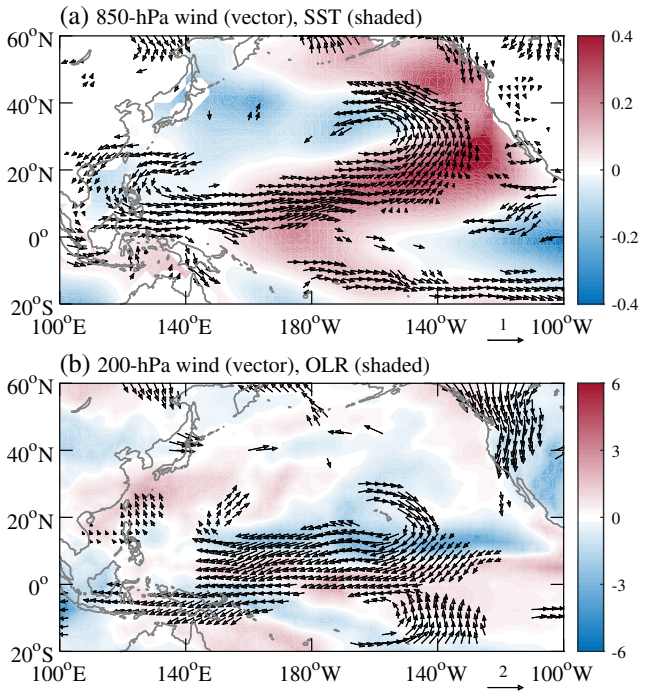

FIGURE 10 Regressions of (a) SST (shaded, K) and 850 hPa wind ($m \cdot s^{-1}$; vector) and (b) OLR ($W\,m^{-2}$; shaded) and 200 hPa wind ($m \cdot s^{-1}$; vector) during JJASON after removing the Niño 3.4 signal. Black vectors show winds significant above the 0.1 level [Colour figure can be viewed at wileyonlinelibrary.com]

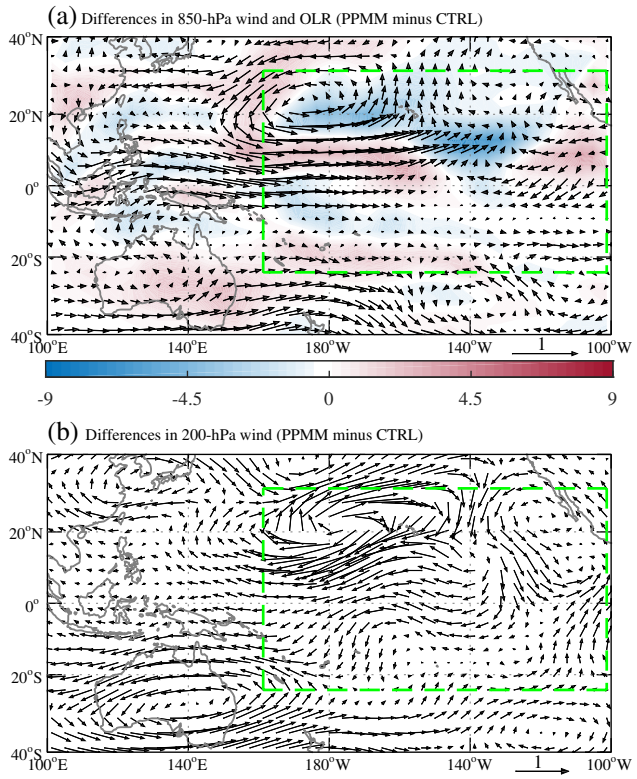

FIGURE 11 (a) Differences in 850 hPa wind ($m \cdot s^{-1}$; vector) and OLR ($W \cdot m^{-2}$; shaded), and (b) 200 hPa wind ($m \cdot s^{-1}$) during JJASON between the PPMM and CTRL experiments with CAM-5.3 (PPMM minus CTRL). The dashed rectangle denotes the PMM region [Colour figure can be viewed at wileyonlinelibrary.com]

predicting landfalling TC frequency in China. The performance of the PMM index in statistical prediction models is evaluated in this section. Potential predictors contain Niño 3.4 index, EMI, SSTG between the tropical Indian Ocean and the western Pacific warm pool, TNA SST, and the PMM index. Two regression models are developed with and without the PMM index using the data during 1977–2015. A stepwise regression method is employed to select significant predictors. If excluding the PMM index in the pool of potential predictors, EMI and Niño 3.4 index (NINO34) are selected as significant predictors to build regression Equation 1. If including the PMM index in the pool of potential predictors, only the PMM index is selected as a significant predictor to build regression Equation 2.

$$y = 5.86 + 2.26 \times \mathrm{EMI} - 0.95 \times \mathrm{NINO34}, \quad (1)$$

$$y = 5.75 + 0.28 \times \mathrm{PMM}. \quad (2)$$

The data during 2016–2018 are then used for independent verification and the results are shown in Table 3. A total of 25 landfalling TCs in China were observed during the 3 years. The regression models without and with the PMM index predict 18.2 and 20.1 landfalling TCs in China, respectively. The use of the PMM index can reduce the prediction error by 1.9, which is equivalent to a decrease in the percentage error of 7.6%. This result demonstrates that the PMM index can be employed to improve the seasonal prediction of landfalling TC frequency in China.

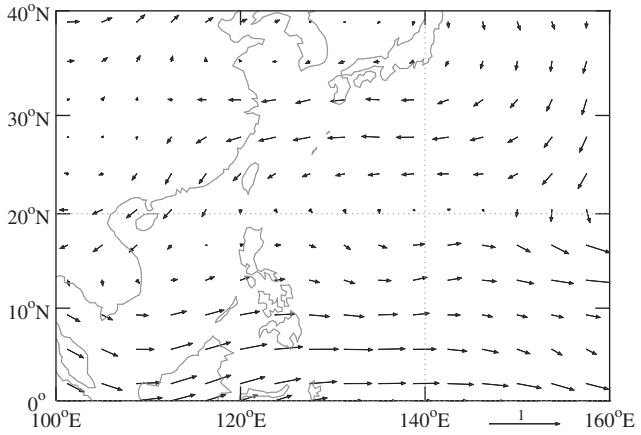

FIGURE 12 Difference in steering flow (850–500 hPa mean winds, $m\ s^{-1}$) during JJASON between the PPMM and CTRL experiments with CAM-5.3 (PPMM minus CTRL)

Regression model	Observed	Predicted	Error	Percentage error
Without the PMM index	25	18.2	−6.8	−27.2%
With the PMM index	25	20.1	−4.9	−19.6%

TABLE 3 Observed and predicted landfalling TC frequency in China as well as the errors during 2016–2018 with and without the PMM index in the regression models

6 | CONCLUDING REMARKS

The impact of PMM on the occurrence of TC landfalls in China and its physical mechanisms have been investigated for the first time. We have identified a significant positive correlation between the PMM index and frequency of TCs landfalling in China during JJASON. During the positive PMM phase, the anomalous off-equatorial heating over the eastern North Pacific can induce anomalous low-level cyclonic flow and upper-level anticyclonic flow over most of the main development region in the WNP via a Gill-type Rossby wave response. The associated larger low-level relative vorticity and weaker wind shear are favourable for the genesis of more TCs *in situ*. The anomalous easterly steering flow in the north flank of anomalous low-level cyclonic flow can lead more TCs to travel westward/northwestward and make landfall in China. The above physical mechanism for the influence of PMM on favourable large-scale circulation for TC landfalls in China during JJASON has been well reproduced by NCAR CAM-5.3.

This study highlights the PMM index as a valuable physically based factor for predicting landfalling TC frequency in China in statistical models. Therefore, incorporating the PMM index into current statistical or statistical-dynamical prediction schemes (e.g. Liu and Chan, 2003; Fan, 2009; Goh and Chan, 2010; Sun and Ahn, 2011; Geng *et al.*, 2016; Zhang *et al.*, 2016c; 2017) has a great potential for improving seasonal prediction of TC landfalls in China. The PMM index is strongly recommended to be used by operational agencies providing official seasonal forecasts of landfalling TC frequency in China.

ACKNOWLEDGEMENTS

The NCEP/NCAR reanalysis, ERSST V4, and OLR data, and the PMM and Niño 3.4 indices are provided by the NOAA/OAR/ESRL PSL from their website at https://psl.noaa.gov/. The ENSO modoki index is provided by the JAMSTEC at http://www.jamstec.go.jp/virtualearth/general/en/index.html. TC best track dataset is provided by the CMA Shanghai Typhoon Institute at http://tcdata.typhoon.org.cn/en/. We appreciate the insightful comments from two anonymous reviewers. This study was supported by the National Key Research and Development Program of China (Grant No. 2019YFC1510400), the National Natural Science Foundation of China (Grant No. 41930967, 41575078, 41975054), and the Strategic Priority Research Program of the Chinese Academy of Sciences (Grant No. XDA20100304).

ORCID

Wei Zhang https://orcid.org/0000-0001-8134-6908

REFERENCES

Camargo, S.J., Emanuel, K.A. and Sobel, A.H. (2007) Use of a genesis potential index to diagnose ENSO effects on tropical cyclone genesis. *Journal of Climate*, 20, 4819–4834.

Camp, J., Roberts, M.J., Comer, R.E., Wu, P.L., MacLachlan, C., Bett, P.E., Golding, N., Toumi, R. and Chan, J.C.L. (2019) The western Pacific subtropical high and tropical cyclone landfall: seasonal forecasts using the Met Office GloSea5 system. *Quarterly Journal of the Royal Meteorological Society*, 145(718), 105–116.

Chan, J.C.L. and Gray, W.M. (1982) Tropical cyclone movement and surrounding flow relationships. *Monthly Weather Review*, 110, 1354–1374.

Chiang, J.C.H. and Vimont, D.J. (2004) Analogous Pacific and Atlantic meridional modes of tropical atmosphere–ocean variability. *Journal of Climate*, 17, 4143–4158.

Elsner, J.B. and Liu, K.B. (2003) Examining the ENSO-typhoon hypothesis. *Climate Research*, 25, 43–54.

Emanuel, K.A. (1988) The maximum intensity of hurricanes. *Journal of the Atmospheric Sciences*, 45, 1143–1155.

Emanuel, K.A. and Nolan, D.S. (2004) Tropical cyclone activity and global climate. *Preprints*. In: *26th Conference on Hurricanes and Tropical Meteorology, Miami, FL*. Miami, FL: American Meteorology Society, pp. 240–241.

Fan, K. (2009) Seasonal forecast model for the number of tropical cyclones to make landfall in China. *Atmospheric Oceanic Science Letters*, 2, 251–254.

Gao, S., Chen, Z. and Zhang, W. (2018a) Impacts of tropical North Atlantic SST on western North Pacific landfalling tropical cyclones. *Journal of Climate*, 31, 853–862.

Gao, S., Zhu, L., Zhang, W. and Chen, Z. (2018b) Strong modulation of the Pacific Meridional Mode on the occurrence of intense tropical cyclones over the western North Pacific. *Journal of Climate*, 31, 7739–4479.

Geng, H., Shi, D., Zhang, W. and Huang, C. (2016) A prediction scheme for the frequency of summer tropical cyclone landfalling over China based on data mining methods. *Meteorological Applications*, 23, 587–593.

Gill, A.E. (1980) Some simple solutions for heat-induced tropical circulation. *Quarterly Journal of the Royal Meteorological Society*, 106, 447–462.

Goh, A.Z.C. and Chan, J.C.L. (2010) An improved statistical scheme for the prediction of tropical cyclones making landfall in south China. *Weather and Forecasting*, 25, 587–593.

Hong, C.C., Lee, M.Y., Hsu, H.H. and Tseng, W.L. (2018) Distinct influences of the ENSO-like and PMM-like SST anomaly on the mean TC genesis location in the western North Pacific: the 2015 summer as an extreme example. *Journal of Climate*, 31, 3049–3059.

Huang, B., Banzon, V.F., Freeman, E., Lawrimore, J., Liu, W., Peterson, T.C., Smith, T.M., Thorne, P.W., Woodruff, S.D. and Zhang, H.M. (2015) Extended Reconstructed Sea Surface Temperature version 4 (ERSST.v4). Part I: Upgrades and intercomparison. *Journal of Climate*, 28, 911–930.

Hurrell, J.W., Holland, M.M., Gent, P.R., Ghan, S., Kay, J.E. and Kushner, P.J. (2013) The Community Earth System Model: a framework for collaborative research. *Bulletin of the American Meteorological Society*, 94, 1339–1360.

Kalnay, E, Kanamitsu, M., Kistler, R., Collins, W., Deaven, D., Gandin, L., Iredell, M., Saha, S., White, G., Woollen, J., Zhu, Y., Chelliah, M., Ebisuzaki, W., Higgins, W., Janowiak, J., Mo, K.C., Ropelewski, C., Wang, J., Leetmaa, A., Reynolds, R., Jenne, R. and Joseph, D. (1996) The NCEP/NCAR 40-year reanalysis project. *Bulletin of the American Meteorological Society*, 77, 437–472.

Liebmann, B. and Smith, C.A. (1996) Description of a complete (interpolated) outgoing longwave radiation dataset. *Bulletin of the American Meteorological Society*, 77, 1275–1277.

Liu, K.S. and Chan, J.C.L. (2003) Climatological characteristics and seasonal forecasting of tropical cyclones making landfall along the south China coast. *Monthly Weather Review*, 131, 1650–1662.

Neale, R.B., Chen, C.-C., Conley, A. J., Garcia, R., Morrison, H., Cameron-Smith, P., Collins, W.D., Iacono, M.J., Easter, R.C., Ghan, S.J., Liu, X., Rasch, P.J. and Taylor, M.A. (2012) *Description of the NCAR Community Atmosphere Model (CAM 5.0)*. NCAR Technical Note NCAR/TN-486+STR. Available at: http://www.cesm.ucar.edu/models/cesm1.0/cam/docs/description/cam5_desc.pdf.

Sun, J. and Ahn, J.B. (2011) A GCM-based forecasting model for the landfall of tropical cyclones in China. *Advances in Atmospheric Sciences*, 28, 1049–1055.

Stuecker, M.F. (2018) Revisiting the Pacific Meridional Mode. *Scientific Reports*, 8, 3216.

Trenberth, K.E. (1997) The definition of El Niño. *Bulletin of the American Meteorological Society*, 78, 2771–2777.

Velden, C.S. and Leslie, L.M. (1991) The basic relationship between tropical cyclone intensity and the depth of the environmental steering layer in the Australian region. *Weather and Forecasting*, 6, 244–253.

Wang, B., Xiang, B. and Lee, J.Y. (2013) Subtropical high predictability establishes a promising way for monsoon and tropical storm predictions. *Proceedings of the National Academy of Sciences of the USA*, 110, 2718–2722.

Wang, L. and Chen, G. (2018a) Impact of the spring SST gradient between the tropical Indian Ocean and western Pacific on landfalling tropical cyclone frequency in China. *Advances in Atmospheric Sciences*, 35, 682–688.

Wang, L. and Chen, G. (2018b) Relationship between South China Sea summer monsoon onset and landfalling tropical cyclone frequency in China. *International Journal of Climatology*, 38, 3209–3214.

Wu, M.C., Chang, W.L. and Leung, W.M. (2004) Impacts of El Niño–Southern Oscillation events on tropical cyclone landfalling activity in the western North Pacific. *Journal of Climate*, 17, 1419–1428.

Wu, Y.K., Hong, C.C. and Chen, C.T. (2018) Distinct effects of the two strong El Niño events in 2015–2016 and 1997–1998 on the western North Pacific monsoon and tropical cyclone activity: role of subtropical eastern North Pacific warm SSTA. *Journal of Geophysical Research: Oceans*, 123, 3603–3618.

Ying, M., Zhang, W., Yu, H., Lu, X., Feng, J., Fan, Y., Zhu, Y. and Chen, D. (2014) An overview of the China Meteorological Administration tropical cyclone database. *Journal of Atmospheric and Oceanic Technology*, 31, 287–301.

Yu, J., Xue, H. and Song, J. (2017) Tropical cyclone potential hazard in southeast China and its linkage with the East Asian westerly jet. *Asia-Pacific Journal of Atmospheric Sciences*, 53, 295–304.

Zhan, R., Wang, Y. and Liu, Q. (2017) Salient differences in tropical cyclone activity over the western North Pacific between 1998 and 2016. *Journal of Climate*, 30, 9979–9997.

Zhang, C., Hu, C., Huang, G., Yao, C., Zheng, Z., Wang, T., Wu, Z., Yang, S. and Chen, D. (2019) Perspective on landfalling frequency and genesis location variations of southern China typhoon during peak summer. *Geophysical Research Letters*, 46, 6830–6838.

Zhang, Q., Wu, L. and Liu, Q. (2009) Tropical cyclone damages in China 1983–2006. *Bulletin of the American Meteorological Society*, 90, 489–495.

Zhang, W., Graf, H.F., Leung, Y. and Herzog, M. (2012) Different El Niño types and tropical cyclone landfall in East Asia. *Journal of Climate*, 25, 6510–6523.

Zhang, W., Vecchi, G.A., Murakami, H., Delworth, T., Wittenberg, A.T., Rosati, A., Underwood, S., Anderson, W., Harris, L., Gudgel, R., Lin, S.J., Villarini, G. and Chen, J.H. (2016a) Improved simulation of tropical cyclone responses to ENSO in the western North Pacific in the high-resolution GFDL HiFLOR coupled climate model. *Journal of Climate*, 29, 1391–1415.

Zhang, W., Vecchi, G.A., Murakami, H., Villarini, G. and Jia, L. (2016b) The Pacific meridional mode and the occurrence of tropical cyclones in the western North Pacific. *Journal of Climate*, 29, 381–398.

Zhang, W., Villarini, G., Vecchi, G.A., Murakami, H. and Gudgel, R. (2016c) Statistical-dynamical seasonal forecast of western North Pacific and East Asia landfalling tropical cyclones using the high-resolution GFDL FLOR coupled model. *Journal of Advances in Modeling Earth Systems*, 8, 538–565.

Zhang, W., Vecchi, G.A., Villarini, G., Murakami, H., Gudgel, R. and Yang, X. (2017) Statistical–dynamical seasonal forecast of western North Pacific and East Asia landfalling tropical cyclones using the GFDL FLOR coupled climate model. *Journal of Climate*, 30, 2209–2232.

Zhang, W. and Villarini, G. (2019) Seasonal forecasting of western North Pacific tropical cyclone frequency using the North American multi-model ensemble. *Climate Dynamics*, 52, 5985–5997.

Zhou, X., Lu, R. and Chen, G. (2018) Impact of interannual variation of synoptic disturbances on the tracks and landfalls of tropical

cyclones over the western North Pacific. *Advances in Atmospheric Sciences*, 35, 1469–1477.

Zhou, X. and Lu, R. (2019) Interannual variability of the tropical cyclone landfall frequency over the southern and northern regions of East Asia in Autumn. *Journal of Climate*, 32, 8677–8686.

How to cite this article: Gao S, Zhu L, Zhang W, Shen X. Impact of the Pacific Meridional Mode on landfalling tropical cyclone frequency in China. *Q J R Meteorol Soc*. 2020;1–11.
https://doi.org/10.1002/qj.3799